Pressure-induced large increase of Curie temperature of the van der Waals ferromagnet VI_3

J. Valenta,[1,2] M. Kratochvílová,[1] M. Míšek,[3] K. Carva,[1] J. Kaštil,[3] P. Doležal,[1] P. Opletal,[1] P. Čermák,[1] P. Proschek,[1] K. Uhlířová,[1] J. Prchal,[1] M. J. Coak,[4,5] S. Son,[6,7,8] J-G. Park,[6,7,8] and V. Sechovský[1]

[1]*Charles University, Faculty of Mathematics and Physics, Department of Condensed Matter Physics, Ke Karlovu 5, 121 16 Prague 2, Czech Republic*

[2]*National Institute for Materials Science, Thermal Energy Materials Group, International Center for Materials Nanoarchitectonics (MANA), 1-2-1, Sengen, Tsukuba, Ibaraki 305-0047, Japan*

[3]*Institute of Physics, Czech Academy of Sciences, Na Slovance 2, 182 21 Prague 8, Czech Republic*

[4]*Department of Physics, University of Warwick, Gibbet Hill Road, Coventry CV4 7AL, United Kingdom*

[5]*Cavendish Laboratory, University of Cambridge, J.J. Thomson Ave, Cambridge CB3 0HE, United Kingdom*

[6]*Center for Quantum Materials, Seoul National University, Seoul 08826, Republic of Korea*

[7]*Center for Correlated Electron Systems, Institute for Basic Science, Seoul 08826, Korea*

[8]*Department of Physics and Astronomy, Seoul National University, Seoul 08826, Korea*

(Received 20 October 2020; revised 15 December 2020; accepted 15 January 2021; published 17 February 2021)

Evolution of magnetism in single crystals of the van der Waals compound VI_3 in external pressure up to 7.3 GPa studied by measuring magnetization and ac magnetic susceptibility is reported. Four magnetic phase transitions, at $T_1 = 54.5$ K, $T_2 = 53$ K, $T_C = 49.5$ K, and $T_{FM} = 26$ K, respectively, have been observed at ambient pressure. The first two have been attributed to the onset of ferromagnetism in specific crystal-surface layers. The bulk ferromagnetism is characterized by the magnetic ordering transition at Curie temperature T_C and the transition between two different ferromagnetic phases T_{FM}, accompanied by a structure transition from monoclinic to triclinic symmetry upon cooling. The pressure effects on magnetic parameters were studied with three independent techniques. T_C was found to be almost unaffected by pressures up to 0.6 GPa whereas T_{FM} increases rapidly with increasing pressure and reaches T_C at a triple point at ≈ 0.85 GPa. At higher pressures, only one magnetic phase transition is observed moving to higher temperatures with increasing pressure to reach 99 K at 7.3 GPa. In contrast, the low-temperature bulk magnetization is significantly reduced by applying pressure (by more than 50% at 2.5 GPa) suggesting a possible pressure-induced reduction of vanadium magnetic moment. First-principles calculations of VI_3 under pressure allow us to ascribe the evolution of T_C with pressure to the reduction of interplanar distance, including the observed slope change at 0.6 GPa. These calculations also describe the associated band gap closing, showing that with a modest compression the material would become metallic. Overall, the large pressure range covered corresponds to a significant change of interplanar interactions. The obtained data thus allow us to shed light on how does the transition between the three-dimensional (3D) and quasi-2D system affect magnetic interactions in the system.

DOI: 10.1103/PhysRevB.103.054424

I. INTRODUCTION

Two-dimensional (2D) van der Waals (vdW) magnetic materials have become the subjects of intensive research activities in recent years, mainly because of their promising application potential for the design of spintronic devices [1–4]. One of these intriguing vdW materials, VI_3, received significant attention from experimentalists [5–14] and theorists [15–27] only recently, despite belonging to the well-studied family of transition metal trihalides. It was stimulated by the breakthrough discovery of 2D ferromagnetism in CrI_3 monolayers [28], whose anisotropy allows one to overcome the effect of the Mermin-Wagner theorem. The studies on VI_3 rapidly appearing in a short time brought numerous surprising experimental results, especially on crystal structures, magnetic phase transitions, and their evolution in external pressure. Most experimental works agreed on the structural transition from the trigonal symmetry to a monoclinic one upon cooling through the transition temperature $T_s \approx 79$ K [5,6,8–10]. Such a transition from a higher to a lower crystal symmetry with decreasing temperature contrasts with the behavior of CrI_3, which has a monoclinic structure at room temperature. It is then transformed into a trigonal structure when cooled below 220 K [29]. The controversy concerning the VI_3 room-temperature crystal structure is based on a series of experimental works reporting contradictory results: Kong *et al.* [6] have reported trigonal $R\bar{3}$ structure at room temperature with structural transition below $T_s = 78$ K. Son *et al.* [5] observed lowering of the crystal symmetry with cooling from the trigonal $P\bar{3}1c$ structure to a monoclinic $C2/c$. Detailed crystal structure study by Doležal *et al.* [9] has confirmed the *R-3* crystal structure at room temperature in agreement with Kong [6]. The room temperature trigonal

structure was later confirmed also by data from a synchrotron experiment [11].

The consensus in VI_3 is on the magnetic phase transition from paramagnetic (PM) to a ferromagnetic (FM) state at Curie temperature $T_C \approx 50$ K. A strong anisotropy with a high anisotropy field (>9 T at 2 K) leads to a high coercive field $\mu_0 H_c \approx 1$ T at 2 K in a magnetic field applied parallel to the c axis [5–7,10,11]. It contrasts with a much lower anisotropy field (≈ 3 T at 2 K) and soft ferromagnetism observed in CrI_3 [29].

Subsequent studies revealed that magnetism in VI_3 is more complicated than initially believed. Gati, *et al.* [8] reported that VI_3 undergoes another magnetic phase transition at 36 K (referred to as $\approx T_{FM2}$) between two ferromagnetically ordered phases. Two magnetically ordered V sites were detected at the lowest temperatures ($T < 36$ K) while there is only one magnetically ordered V site at temperatures between 36 K and T_C by ^{51}V and ^{127}I NMR spectroscopy [7]. The low-temperature x-ray diffraction indicated that this transition is associated with the reported transition between the monoclinic and triclinic structure at 32 K upon cooling [9].

Measurements of magnetic parameters of materials exposed to external pressure provide valuable information about the character of exchange interactions and magnetism's dimensionality. The application of hydrostatic pressure leads to reducing the interatomic distances in proportion to the corresponding direction's compressibility. Consequently, exchange integrals, the hierarchy of exchange interactions, and magnetic moments are modified, and the critical parameters like T_C are continuously tuned by varying applied pressure. Natural materials' compressibility is often anisotropic, particularly in layered vdW crystal structures with different intralayer and interlayer bonding types. Two-dimensional vdW materials can serve as excellent examples of anisotropic compressibility under hydrostatic pressure, as it is several times larger within the parallel van der Waals bonds than in perpendicular directions [30–34]. When sufficient pressure is applied in a vdW material, usually an insulator, it may undergo a Mott insulator-metal transition. Besides a large change of electrical conductivity, this transition is usually accompanied by a significant change in magnetic behavior [35,36].

In VI_3, the first measurements of magnetic parameters in hydrostatic pressure [5] showed that T_C remains almost intact in low pressures up to 0.6 GPa. The increase of T_C at 1 GPa has been ascribed to tuning the VI_3 dimensionality away from two dimensions. The subsequent detailed measurements of temperature dependences of specific-heat and magnetization under various pressures [8] shed new light on the unusual pressure dependence of T_C. This study confirmed that T_C (assigned in Ref. [8] as T_{FM1}) is almost unaffected by hydrostatic pressure up to 0.6 GPa and revealed that T_{FM2} increases significantly with increasing pressure, so that the related transition merges with the FM transition at T_C in the pressure of ≈ 0.6 GPa. T_C has been reported to increase above this pressure reaching ≈ 69 K in $p = 2.08$ GPa. Some theoretical papers predicted a considerable increase of T_C of the VI_3 monolayer under a tensile strain or having iodine deficiency [16,17,27].

Herein we report on the evolution of magnetism in VI_3 in external pressures up to 7.3 GPa, which we found by detailed measurements of ac magnetic susceptibility (real part χ' and imaginary part χ'') and low-field magnetization depending on temperature (T). We confirmed the existence of the two magnetic phase transitions reported in the literature [5,6,8,10,11]: (a) a PM ↔ FM1 transition at $T_C = 49.5$ K, (b) a transition between two ferromagnetic states FM1 and FM2 at $T_{FM} = 26$ K. The temperatures T_C and T_{FM} in our nomenclature correspond to T_{FM1} and T_{FM2}, respectively, introduced by Gati *et al.* [8]. The T_{FM} transition is most likely accompanied by the monoclinic ↔ triclinic structural transition [9].

Moreover, we observed visible peaks at temperatures $T_1 = 54.5$ K and $T_2 = 53$ K, on $\chi'(T)$, $\chi''(T)$, and $\partial M/\partial T$ vs T curves that allow understanding of the multistep anomaly observed in $M(T)$ dependence near T_C [5]. Considering results of the analysis of exchange interactions and theoretical density functional theory (DFT) calculations of magnetism in VI_3 [16,27] we suggest that these anomalies reflect the onset of ferromagnetism in two types of surface layers of the VI_3 single crystal that are suffering from iodine deficiency or some lattice defects mimicking intralayer tensile strain. In this scenario, the intrinsic bulk ferromagnetism in VI_3 exists only at temperatures below T_C.

The characteristic temperatures T_1, T_2 and T_C were found nearly intact by $p < 0.6$ GPa but T_{FM} increases strongly with increasing pressure and the FM2 expands in the T-p phase space on account of FM1. The FM1 phase is terminated at a triple point at ≈ 0.85 GPa. At higher pressures, only one ferromagnetic phase exists below T_C, which further increases with increasing p and eventually reaches a high value of 99 K (double value of the ambient-pressure T_C) at 7.3 GPa. On the other hand, the high-field magnetization measured at 2 K decreases rather significantly with increasing pressure up to 2.5 GPa. To support the interpretation of observed results selected first-principles calculations were also performed.

In this work, we tried to understand the origin of the recently observed unusually complex evolution of magnetism in a two-dimensional material, accompanied by crystal structure changes with varying temperatures and high pressure. According to our data, this intriguing change arises from a complex hierarchy of magnetic and magnetoelastic interactions with pressure-induced details of the crystal structure and consequent electronic-structure changes.

II. EXPERIMENTAL DETAILS

The VI_3 single crystals were grown by chemical vapor transport method according to the procedure described by Son *et al.* [5]. The samples had a shape typical for vdW materials, thin plates with some hexagonal-like edges and the c axis perpendicular to the plates at room temperature. Their typical lateral dimensions were up to several millimeters. As the samples degrade and subsequently decompose rather quickly when exposed to air or moisture, they were stored under the inert Ar (6N purity) atmosphere in a glovebox. The contact with air was minimized only on the time of the installation of the samples on the sample holders and in the cryostat which took less than 15 min in all cases. A fresh sample was used for every separate measurement. We omitted samples with many surface defects as they can become a source of degradation.

Magnetization and ac susceptibility data at ambient pressure were obtained utilizing MPMS XL 7T (*Quantum Design*

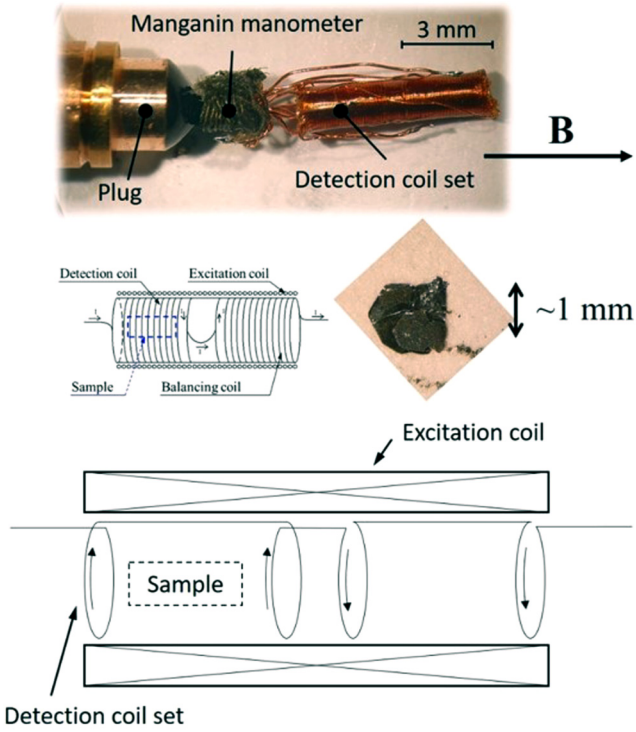

FIG. 1. The pressure experimental setup for measuring the ac susceptibility. Details of the pressure cell are described in the Experimental Details section.

Inc.) using a crystal oriented with the c^* axis ($\equiv$ the surface normal) either parallel or perpendicular to the applied magnetic field. The magnetization behavior under hydrostatic pressures was measured with the same MPMS 7T using two different pressure cells: (a) for pressures up to 1 GPa the "piston-cylinder" pressure cell made from nonmagnetic Cu/Be-alloy [37] with a Daphne 7474 pressure medium [38] and a superconducting lead manometer, determining the pressures directly at low temperatures, (b) for high pressures up to 7.3 GPa, the "turnbuckle"-type diamond anvil cell (DAC) [39]. The cell is built from made-to-order ultrapure Cu/Be alloy, allowing sensitive measurements with an extremely small sample in DAC. Daphne 7575 pressure medium [40] was used, and pressure has been determined at room temperature by a ruby manometer. Due to geometrical constraints of the DAC cell the sample was oriented with the c^* axis aligned to the applied magnetic field in the latter type of experiment.

The hydrostatic pressure influence of the ac susceptibility was measured using a set of homemade miniature coils with Ø of $\approx$ 1.5 mm and length of $\approx$ 6 mm (a primary coil for ac field generation has ~200 turns, secondary one for AC magnetic susceptibility detection having 50 and 50 turns wound in an opposite sense to compensate for the signal of the sample surroundings, see Fig. 1). The coils were connected to a Stanford Research Systems lock-in amplifier, model SR 830 used for AC signal processing while measuring both real (χ') and imaginary (χ'') parts. The coils set fits inside double-layered CuBe/NiCrAl piston-cylinder pressure cell [41,42] used to generate pressures up to ~3.5 GPa (room-temperature value). We used the Daphne oil 7373 [43] as the pressure transmitting medium with a manganin manometer to determine the cell's pressure at room temperature. After cooling down to the base temperature, we calibrated the pressure again using our cell's pressure calibration table. The ac susceptibility measurement was accomplished by a closed cycle refrigerator (*Janis Research Company, LLC/Sumitomo Heavy Industries, Ltd.*). The ambient-pressure specific-heat data were collected in the temperature range 2–300 K in magnetic fields up to 14 T applied along the c^* axis using PPMS-14 (*Quantum Design, Inc.*). The angular dependence of magnetization was measured at 2 K using an MPMS sample rotator.

III. CALCULATION DETAILS

DFT calculations were based on the full-potential linear augmented plane wave method, as implemented in the ELK code [44]. The spin-orbit coupling has been included within the second variational approach. The generalized gradient approximation has been employed. Since the system is known to be a Mott insulator [5,7], Hubbard U has been added to describe electron correlations within the fully localized limit double-counting treatment [45]. For $U = 3.8$ eV, this leads to predicting a bandgap with a size of around 0.6 eV. We covered the full Brillouin zone by sampling about $1000\,k$ points. We have assumed the rhombohedral structure of BiI_3 with experimental lattice parameters [7] $a = 0.6835$ nm and $c_0 = 0.6565$ nm (equilibrium interlayer distance).

To study the effect of pressure by first-principles calculations, we utilize the high anisotropy of compressibility in the vdW materials. And so up to some threshold, the compression takes place mainly perpendicular to the basal plane. We have assumed that the pressure leads to compression of the van der Waals gap within the studied range, while distances between V and I inside a layer remain unchanged.

IV. RESULTS AND DISCUSSION

Before we come to results of our measurements, we note that the c^* axis represents the surface normal corresponding to the *ab* plane which does not have to be identical with the crystallographic c axis in various temperatures. The c^* and c axis are identical in the trigonal structure that is adopted by VI_3 at temperatures above 80 K but they are mutually deflected in the monoclinic and triclinic phases realized at lower temperatures. In particular, the monoclinic angle between the a and c axis $\beta = 90.00^\circ$ at $T \geqslant 80$ K (trigonal phase). In the monoclinic phase, which exists between 79 and 32 K, $\beta \leqslant 90.51^\circ$ (see Fig. 5 in Ref. [9]) that implies the deflection angle between the c^* and c axis $= \beta$-90 $\leqslant 0.51^\circ$. We were not able to determine the space group of the triclinic structure of VI_3 below 32 K from available diffraction data but we could estimate that the angle between the c^* and c is certainly smaller than 1 °. The difference between the corresponding c^* and c axis magnetization data is <0.1%, thus much smaller than the experimental error of the magnetization measurements. Consequently, the c^* and c axis magnetization data can be compared without any special correction.

Figures 2 and 3 show how the magnetic phase transitions VI_3 are manifested in the temperature dependences of specific

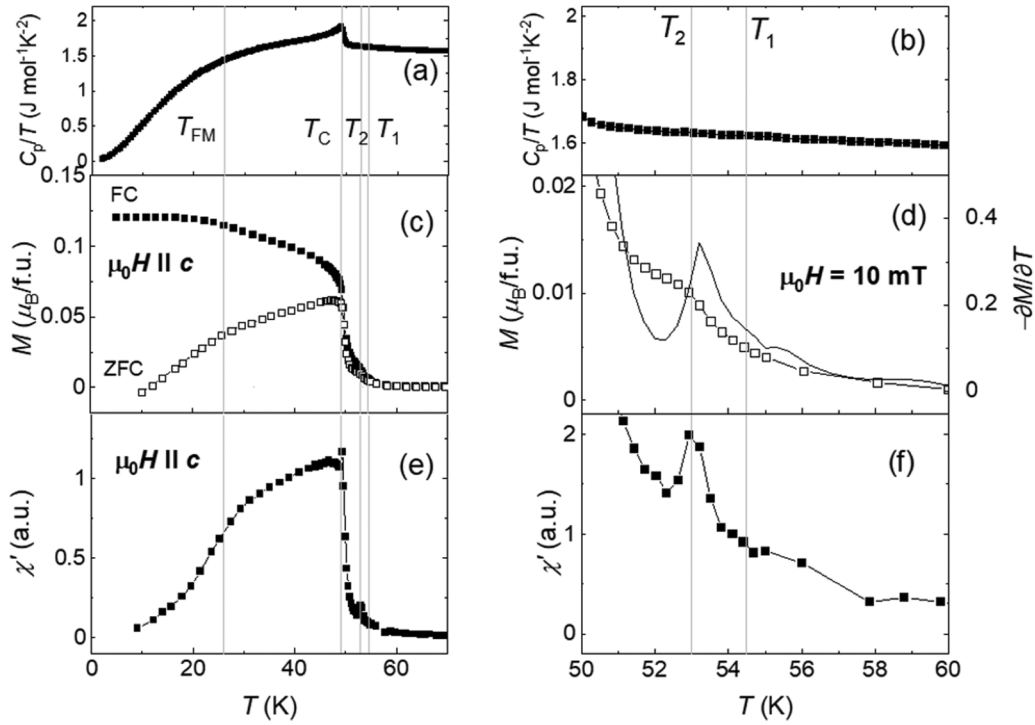

FIG. 2. The left-hand panels corresponding to the *Cp/T* vs *T, M*(*T*), and $\chi'(T)$ plots show a broad temperature range including all the T_1, T_2 T_C, and T_{FM} transitions. The right-hand panels show their magnified images in a narrower temperature range above T_C to see better the T_1 and T_2 related anomalies. Temperature dependences of specific heat (*Cp/T* vs *T* plot) (a),(b); FC and ZFC magnetization in a static magnetic field of 10 mT applied parallel to c^* axis in the FC and ZFC mode, respectively (c), (d) [the dashed line in (d) represents the $-\partial M/\partial T$ vs *T* plot]; real component of the ac magnetic susceptibility χ' for the ac magnetic field applied along the c^* axis (e), (f). The error bars are smaller than the markers. The vertical lines represent the temperatures of the considered magnetic phase transitions.

heat, magnetization in a low static magnetic field, and AC susceptibility. The specific-heat measurement is one of the methods allowing us to determine the critical temperature of magnetic ordering in a bulk material in the absence of a magnetic field. The lambda anomaly manifests a second-order magnetic phase transition of VI_3 at $T_C = 49.5$ K, as shown in Fig. 2(a). The evolution of the C_p/T vs *T* plot with increasing magnetic fields displayed in Fig. 4 is characteristic of ferromagnetic order. The value of T_C determined here is reasonable with results published before [5–7,10,11].

The ferromagnetic transition at T_C appears in the $\chi'(T)$ and $\chi''(T)$ curves as a high and sharp peak just at T_C, and as an inflection point of the steep increase of the low-field $M(T)$ dependences both in the field-cooled (FC) and zero-field-cooled (ZFC) mode upon cooling. The ferromagnetic ordering is accompanied by a distortion of the crystal lattice. It is indicated by the change of slope of the temperature dependence of the angular position of the diffraction peak at T_C [9], in particular, the monoclinic (2 6 21) reflection. We note that the irreversibility between the FC and ZFC $M(T)$ curves is not caused by the spin-glass behavior as the ac susceptibility data are frequency-independent (see Fig. 5). Instead, it comes probably from anisotropic interactions combined with domain physics which plays a dominant role at low fields (the measurement was performed at 10 mT).

Closer inspection of Figs. 2 and 3 reveals small peaks on the $\chi'(T)$,$\chi''(T)$, and $\partial M/\partial T$ vs *T* curves at temperatures above T_C, namely at $T_1 = 54.5$ K and $T_2 = 53$ K. Analogous results were reported by Liu *et al.* [11] and Gati *et al.* [8]. Measuring different samples of the VI_3 crystals we have found that the size of these anomalies is strongly sample dependent (in some cases only the peak at T_2 is visible) but the differences T_1–$T_C = 5$ K and T_2–$T_C = 3.5$ K, respectively, seem to be sample independent. The lack of any response around T_1 and T_2 on the C_p/T vs *T* plots corroborate the idea that the T_1 and T_2 transitions are in fact not intrinsic phenomena in the bulk of the VI_3 crystal. $\partial M/\partial T$ vs *T* plots, $\chi'(T)$, and especially $\chi''(T)$ anomalies at T_1 and T_2 provide strong indications of ferromagnetic transitions in parts of samples.

Theoretical studies within DFT revealed that the hierarchy of exchange interactions in a VI_3 monolayer could be influenced by applying tensile strain [16] or producing iodine deficiency [27] to increase Curie temperature. Considering these results and having in mind that the VI_3 surface rapidly degrades and finally decomposes when exposed to oxygen and moisture, we suggest that two types of surface iodine-poor layers may become ferromagnetic at temperatures (T_1 and T_2, respectively) higher than the T_C of the VI_3 bulk crystal. This is corroborated by the fact that the T_1 transition is not obvious in the measurement with the magnetic field along the c^* axis, unlike the T_2 transition, which is clearly visible in both measured directions [see Figs. 2(f) and 3(f)]. The samples could be exposed to air or different moisture for a slightly different time during the necessary manipulation, and more importantly,

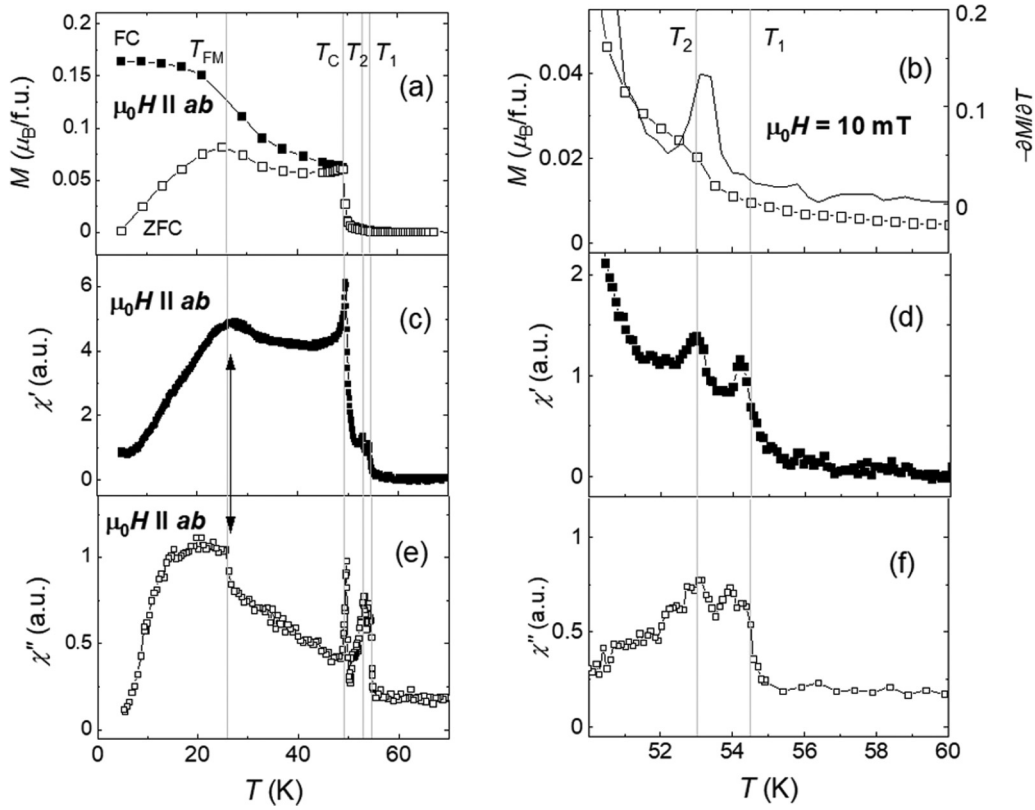

FIG. 3. The left-hand panels corresponding to the $M(T)$, $\chi'(T)$, $\chi''(T)$ plots show a broad temperature range including all the T_1, T_2 T_C, and T_{FM} transitions. The right-hand panels show their magnified images in a narrower temperature range above T_C to see better the T_1- and T_2-related anomalies. The FC and ZFC temperature dependences of magnetization in a static magnetic field of 10 mT applied perpendicular to the c^* axis (a), (b) [the dashed line in (b) represents the $-\partial M/\partial T$ vs T plot); real component of the ac magnetic susceptibility χ' for the ac magnetic field applied perpendicular to the c^* axis (c), (d) and the corresponding imaginary component $\chi''(T)$. The error bars are smaller than the markers. The vertical lines represent the temperatures of the considered magnetic phase transitions.

the samples probably revealed different amount of defects, like cracks, etc., which directly affects the degradation rate of the single crystals.

The C_p/T vs T plot at temperatures below 40 K is very smooth and monotonous, showing no trace of the T_{FM} transition, not even the weak cusp at 36 K observed with a sample in

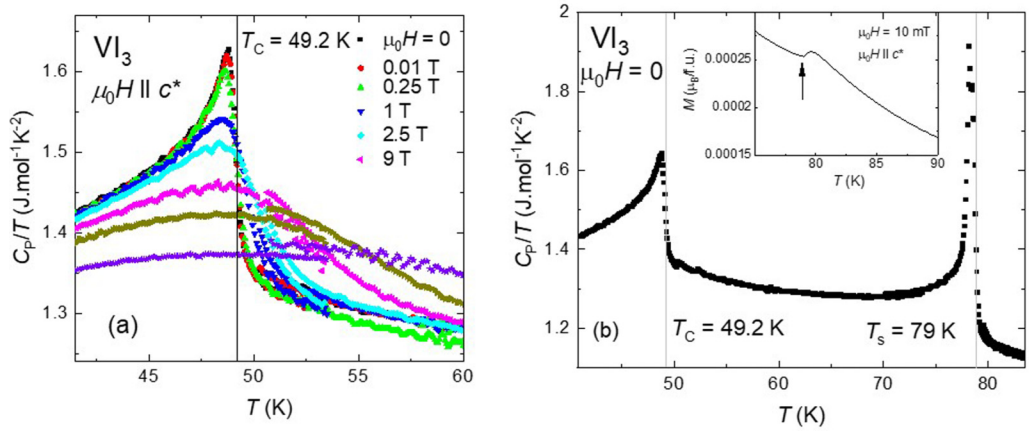

FIG. 4. (a) The λ-shaped anomaly in the temperature dependence of the specific heat of VI_3 in zero magnetic fields reflecting the second-order phase transition at T_C and its evolution with applied magnetic field documenting that it is a transition to the ferromagnetic state below T_C. (b) The ferromagnetic and structural transitions at T_C and T_s, respectively, marked by vertical lines, in the temperature dependence of the specific heat of VI_3 in zero magnetic fields. The inset shows magnetic susceptibility measured along the c^* axis in the temperature region where the structural transition at $T_s = 79$ K can be observed (marked by a vertical arrow).

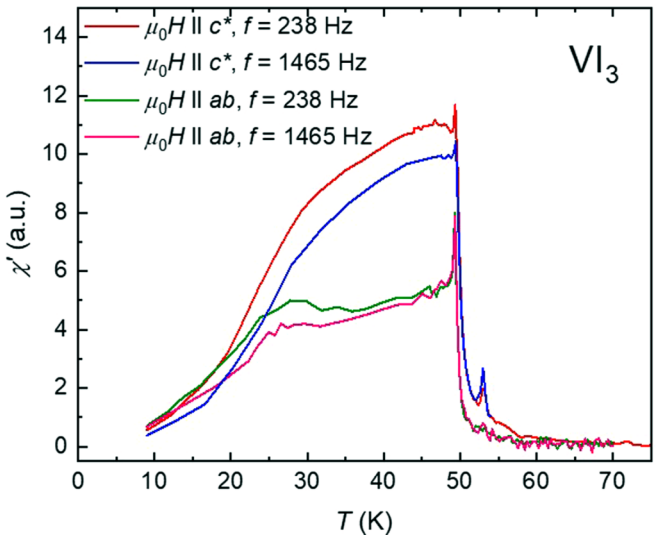

FIG. 5. $\chi'(T)$ dependences measured with the ac magnetic field applied parallel and perpendicular to the c^* axis at two different frequencies.

pressure cell [8]. The characteristic temperature of structural transition was reported at 32 K [9] at which we also cannot find clear indications of a magnetic phase transition in the AC susceptibility data.

On the other hand, the maximum in the $\chi'(T)$ and low-field $M(T)$ curves and particularly the discontinuous step in $\chi''(T)$ dependence at $T_{FM} = 26$ K in fields perpendicular to the c^* axis point to a sudden change of ferromagnetic phase, probably a transition between the two ferromagnetic phases (FM1 existing at temperatures between T_C and T_{FM} and the ground state phase, FM2, below T_{FM}). The evolution of these anomalies with applied hydrostatic pressure and comparison with the magnetic phase diagram presented in Ref. [7] discussed below corroborate this idea.

In Fig. 6, we can see how the $\chi'(T)$ and $\chi''(T)$ dependences are modified by applying hydrostatic pressure in the VI_3 crystals. The positions of features related to T_1, T_2, and T_C appear not to be affected by pressures up to ≈ 0.6 GPa. Then these characteristic temperatures slightly increase with increasing p up to ≈ 0.8 GPa. T_{FM}, on the contrary, increases rapidly with increasing pressure already in the lowest pressures, and for $p \approx 0.8$ GPa, it reaches T_C. For pressures higher than 0.8 GPa, we can see only one anomaly on the $\chi'(T)$ and $\chi''(T)$ curves, respectively. Complete data of the AC-susceptibility measurement can be found in Fig. 7.

The 1-mT $M(T)$ dependences measured in pressures up to 7.3 GPa using the DAC are displayed in Fig. 8. The T_C value was determined as the temperature of the inflection point of the steep $M(T)$ increase with decreasing temperature. The $M(T)$ curve measured in 0.4 GPa exhibits a visible sidestep at ≈ 53 K, which can be understood as a mark of the T_2 transition. Consistent with $\chi'(T)$ data, in which the T_2-transition anomaly does not show up at pressures above 1 GPa, the $M(T)$ curve is smooth at $T > T_C$. The three $M(T)$ curves in pressures $0.78 - 3.5$ GPa are incredibly sharp in the vicinity of T_C (within 1 K), which may signal the first-order transition as also suggested by Gati *et al.* [8]. Temperature dependence

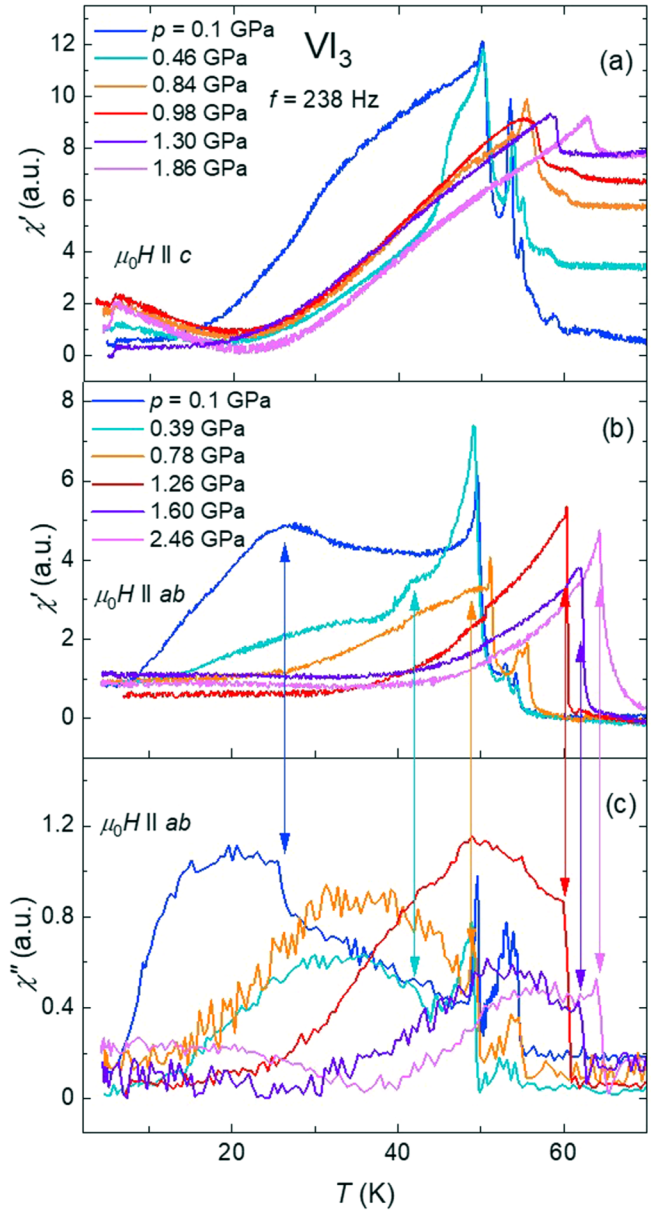

FIG. 6. Selected $\chi'(T)$ dependences for the ac magnetic field applied parallel to the c^* axis (a) and $\chi'(T)$ and $\chi''(T)$ curves measured in the ac field in the ab-plane (b), (c), respectively, on the VI_3 crystals exposed to various hydrostatic pressures. The double-sided arrows indicate the $\chi'(T)$ and $\chi''(T)$ anomalies corresponding to the T_{FM} transitions observed at particular pressures.

of magnetization exposed to hydrostatic pressures to 0.78 GPa can be found in Fig. 9. Pressure dependence of FWHM of the ferromagnetic transition exposed to hydrostatic pressures generated by the DAC is shown in Fig. 10.

The pressure dependences of characteristic temperatures T_1, T_2, T_C, and T_{FM} obtained from data analysis are presented in the schematic T-p phase diagram in Fig. 11. The $T_1(p)$ and $T_2(p)$ lines simultaneously slightly increase the pressure up to ≈ 1 GPa. Since the T_1 and T_2 transitions are not intrinsic magnetic phase transitions of bulk VI_3, they will not be further discussed in the framework of the T-p, the magnetic phase diagram of this compound.

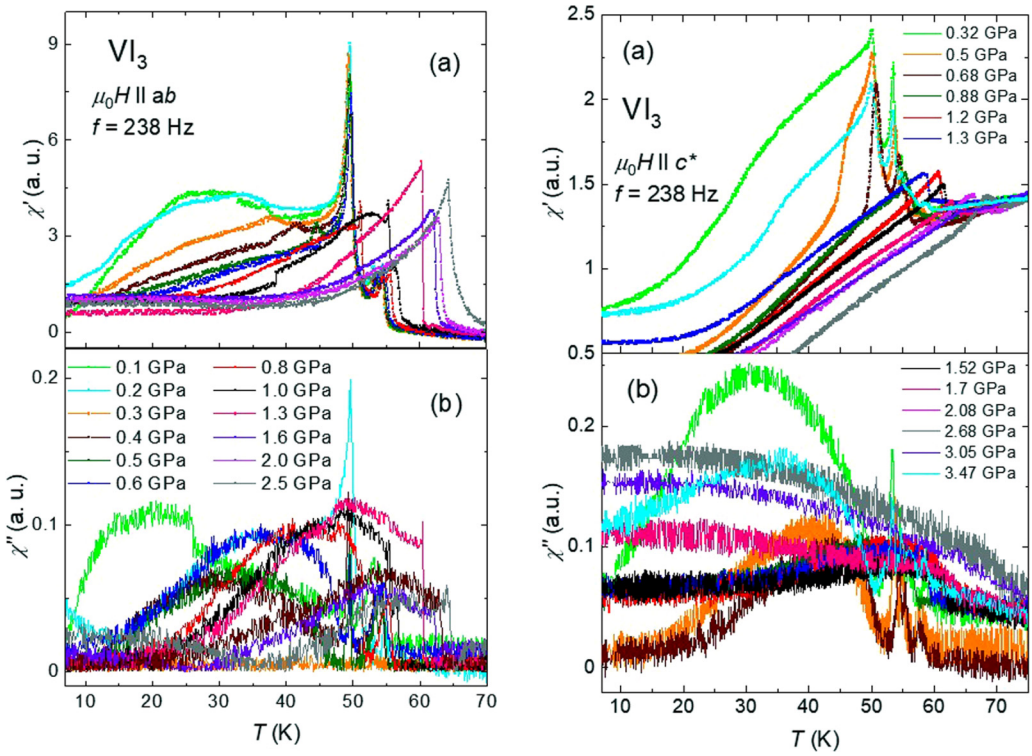

FIG. 7. All real (a) and corresponding imaginary (b) temperature dependences of the ac susceptibility measured with the ac magnetic field ($f = 238$ Hz) applied perpendicular (left panel) and parallel (right panel) to the c^* axis on the VI_3 single crystals exposed to various hydrostatic pressures.

The intrinsic magnetic phases and phase lines in the *T-p* phase space for $p \leqslant 2.08$ GPa derived from data of our AC susceptibility and low-field magnetization data vs temperature are in good agreement with the results of Gati *et al.* [8] who discovered that VI_3 appears in two ferromagnetic phases. The transition between two ferromagnetic phases occurring at a critical temperature is designated in our nomenclature as T_{FM}. When cooled at ambient pressure, VI_3 first undergoes the transition from PM to FM1 state at T_C and then at T_{FM} (<40 K) a transition between two ferromagnetic phases. Our specific-heat, ac-susceptibility, and low-field magnetization data obtained at ambient pressure point to $T_C = 49.5$ K and $T_{FM} = 26$ K (except for specific heat). The Curie temperature does not change significantly below 0.6 GPa, but T_{FM} increases fast with increasing the applied pressure. Consequently, the FM2 phase expands in the *T-p* phase space on account of the FM1 one. $T_C(p)$ and $T_{FM}(p)$ phase lines finally meet at the triple point in pressure p_{TP} near to 0.8 GPa, where the FM1 phase terminates. Although there has been speculation about this point's tricritical nature in the *T-p* phase space [8], supported by the observation of very narrow transitions in our *M*(T) data, we judge that more pressure points would need to be measured to answer this question. Nevertheless, the character of the *T-p* phase space in the vicinity of the triple point suggests a strong coupling of the magnetic and structural degrees of freedom which might be a source of significant magnetocaloric effect. In pressures $p > p_{TP}$, only the phase FM2 exists with the critical temperature labeled as T_C. The character of the magnetization curves for pressures $p > p_{TP}$ becomes second-order-like again which can be, however, affected by the nonhydrostacity of the pressure medium as discussed further. The temperature T_C then further increases with increasing pressure. The evolution of bulk magnetic phases and related phase transitions with pressure up to 2.08 GPa observed in our study is in good agreement with results published by Gati *et al.* [8]. They also showed that the critical temperature of the monoclinic ↔ trigonal structural transition T_s rapidly decreases with applied hydrostatic pressure and the $T_s(p)$ and $T_C(p)$ curves merge at $p_m \approx 1.35$ GPa. That probably means that the ferromagnetic transition at T_C is accompanied by the trigonal ↔ monoclinic or trigonal ↔ triclinic structural transition for $p > p_m$. In contrast, at lower pressures, the monoclinic structure remains preserved at temperatures above T_C up to T_s.

At higher pressures, the $T_C(p)$ almost saturates around 2.5 GPa but resumes considerable growth in pressures above 3.4 GPa. Finally, at the maximum pressure of our experiment, 7.3 GPa, T_C reaches 99 K. This is the double value of the ambient-pressure T_C value that corresponds to the average value of $\partial ln T_C/\partial p = 0.137\,\mathrm{GPa}^{-1}$.$VI_3$ exhibits, to our best knowledge, the largest pressure-induced increase of T_C among the 2D van der Waals ferromagnets. Pressure studies of these materials revealed increasing T_C only in case of CrI_3 [46], which exhibits a 7% increase of T_C from the ambient-pressure value of 60.5 to 65 K in 1 GPa ($\partial \ln T_C/\partial p = 0.074\,\mathrm{GPa}^{-1}$). In the other three studied vdW ferromagnets CrB_3 [47], $Cr_2Ge_2Te_6$ [48] and Fe_3GeTe_2 [49], the hydrostatic pressure causes reduction of T_C. The large pressure-induced increase of Curie temperature of VI_3 belongs to the most important results of this study.

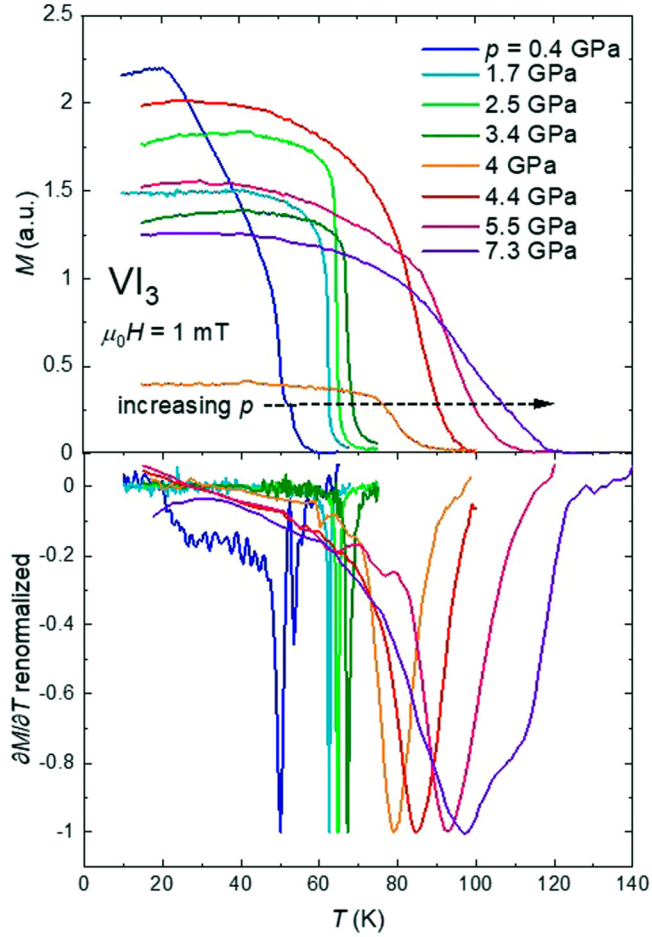

FIG. 8. Temperature dependences of magnetization in a static magnetic field of 1 mT applied parallel to the c^* axis of a VI_3 single crystal exposed to high pressures generated by DAC. The bottom panel shows the renormalized derivation of magnetization used to determine the positions of the transition temperatures T_C.

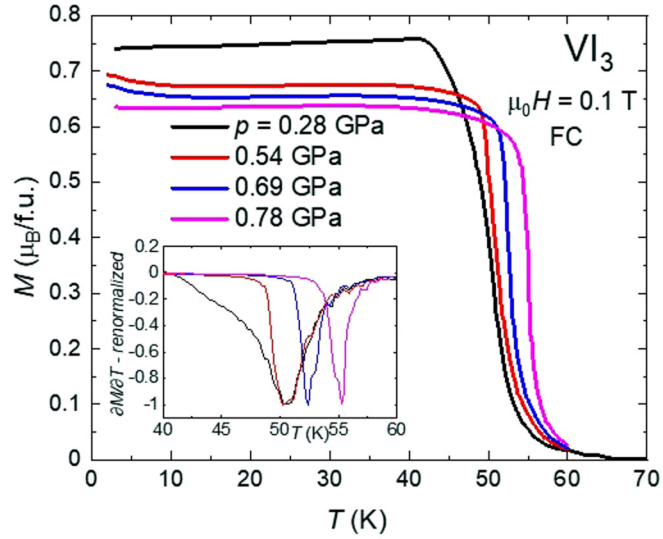

FIG. 9. Temperature dependence of magnetization in a static magnetic field of 100 mT in the field-cooled mode applied along the c^* axis of a VI_3 single crystal exposed to hydrostatic pressures generated by the piston-cylinder cell. The inset shows the renormalized derivation of magnetization $\partial M/\partial T$.

The accelerated increase of T_C with increasing pressure in the 3.4–4 GPa pressure range can be due to the non-hydrostaticity of the pressure transmitting medium (Daphne 7575) in DAC in the high-pressure range. In this case, partially uniaxial stress along the c^* axis is expected. This result appears to be consistent with the calculated effect of the c^* axis compression on the exchange integral shown in Fig. 12.

First-principles calculations have been employed to examine the effect of lattice compression on magnetic interactions, which control the Curie temperature. Intralayer exchange interactions are characterized by the energy difference between the FM state and the Néel antiferromagnet (NAFM, Fig. 13), E_{FM}–E_{NAFM}, which in terms of nearest-neighbor interactions between V atoms corresponds to the first- and third-nearest neighbors [27]. We found these interactions are strong, E_{FM}–$E_{NAFM} = 71$ meV, in agreement with another calculation where these values correspond to $T_C \sim 240$ K in layers [27]. These robust interactions originate from the nearly 90° FM superexchange [50]. They are not affected by the vdW gap's compression up to a specific limit. The interlayer interactions are described by $J_z = E_{FM}$–E_{zAFM}, where zAFM corresponds to antiferromagnetically ordered FM layers (see Fig. 13). This coupling is much weaker, $J_z = 5$ meV for the equilibrium structure, similar to layered Cr compounds [51]. It is thus reasonable to expect that in bulk, the T_C will be affected mainly by the interlayer interaction J_z. The value of this interaction as a function of the interlayer distance c is plotted in Fig. 12. For small compressions it remains almost constant, while it grows approximately linearly for larger ones. It shows that the vdW gap's compression leads to the observed pressure dependence of T_C. This shows that

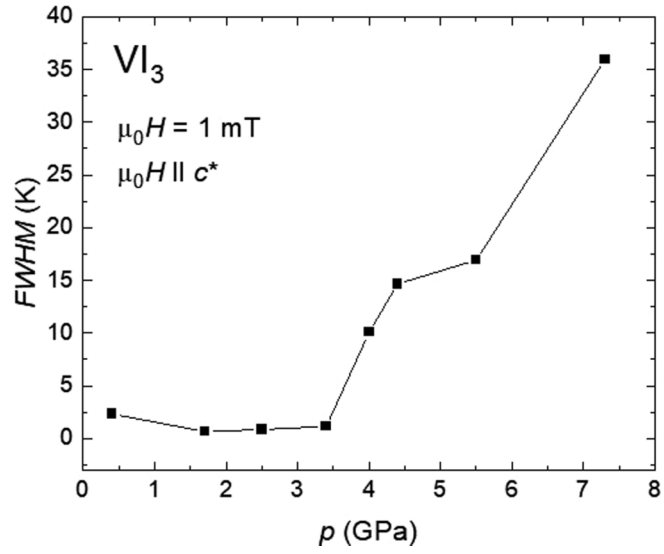

FIG. 10. Pressure dependence of FWHM of the ferromagnetic transition at T_C determined from the derivation of magnetization $\partial M/\partial T$, measured in a static magnetic field of 1 mT applied along the c^* axis of a VI_3 single crystal exposed to hydrostatic pressures generated by the DAC.

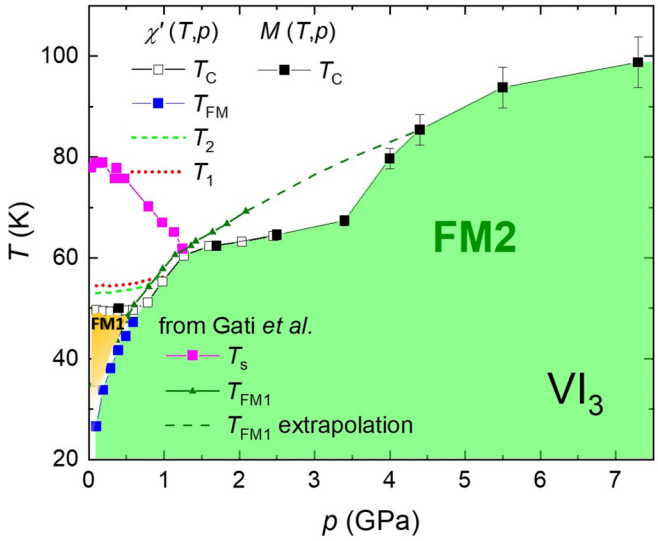

FIG. 11. Temperature-pressure (T-p) magnetic phase diagram of VI_3 derived from results of the ac and DC magnetic susceptibility magnetization measurements measured with a sample in a piston-cylinder and DAC pressure cell, respectively. The meaning of the critical temperatures T_1, T_2, T_C, and T_{FM}, as well as the phases FM1 and FM2 is explained in the text. The comparison of data sets measured by DAC and two different piston-cylinder cells, respectively, in the overlapping pressure interval ($\leqslant 2.5$ GPa) proves that the pressures accomplished by the two different types of cells are coinciding. We added to the phase diagram the pressure evolution of the structure transition T_s and the ferromagnetic transition T_{FM1} together with its extrapolation for higher pressures; both data sets are taken from Gati *et al.* [8].

in the calculation the vdW gap's compression leads to the experimentally observed pressure dependence of T_C in the region 0–1.5 GPa. We have obtained this result without assuming the suggested onset of interplanar interactions starting from some threshold pressure value. We have examined also the case of gap extension, and the calculated J_z exhibits renewed decrease. This implies that when going in the opposite direction, from a smaller vdW gap to a larger one, we can indeed observe a transition from 3D to 2D behavior, but upon reaching the equilibrium value this process is not yet complete, only temporarily slowed down. There is also no need to consider pressure-induced modification of the structure of individual planes, which was predicted to lead to a T_C increase too [16,17,27]. Although after passing a specific threshold pressure value, this may become important too.

The low-temperature magnetization data measured on VI_3 single crystals in magnetic fields parallel and perpendicular to the *ab*-plane, respectively, provide information on a magnetocrystalline anisotropy [5,6,10]. In contrary to the uniaxial anisotropy in CrI_3 [29], the situation in VI_3 appears to be more complicated. In this case, the anisotropy is strong, and the easy magnetization direction is undoubtedly not perpendicular to the *ab* plane. However, the c^*-axis magnetization in fields > 2 T is considerably larger than the corresponding values in perpendicular direction [5,6,10]. Kong *et al.* [6] pointed out the specific $M(H)$ behavior can be understood in terms of V magnetic moments canted from the c^* axis. We measured the angular dependence of the 5 T magnetization in the $c^* - a$ plane at 2 K.

The $M(\phi)$ dependence shown in Fig. 14 has a minimum for $H \perp c^*$, a local minimum for $H // c^*$, and a maximum for the angle of canting $\phi = 40^\circ$ from the c^* axis. Similar results were reported by Yan *et al.* [10]. In the simplest case of collinear V magnetic moments canted by 40 ° from the c^* axis, one can consider that the $M // c^*$ and $M \perp c^*$ data represent their projections on the c^* axis and the *ab* plane. The difference between VI_3 and CrI_3 may originate from the fact that CrI_3 has a closed t_{2g} shell, unlike VI_3.

The thermomagnetic curves and hysteresis loops of VI_3 single crystals were measured in various pressures in magnetic fields applied in two principal directions, i.e., parallel and perpendicular to the c^* axis at selected temperatures. The $M(H)$ hysteresis loops (see Fig. 15 in Appendix) show that in both cases, the high-field magnetization considerably decreases with increasing pressure already in relatively small pressures (<1 GPa), which indicates the pressure-induced reduction of the V moment (by $\sim$ 14% between 0.1 and 0.74 GPa). This measurement was done with the 1 GPa piston-cylinder cell. The temperature evolution of the hysteresis

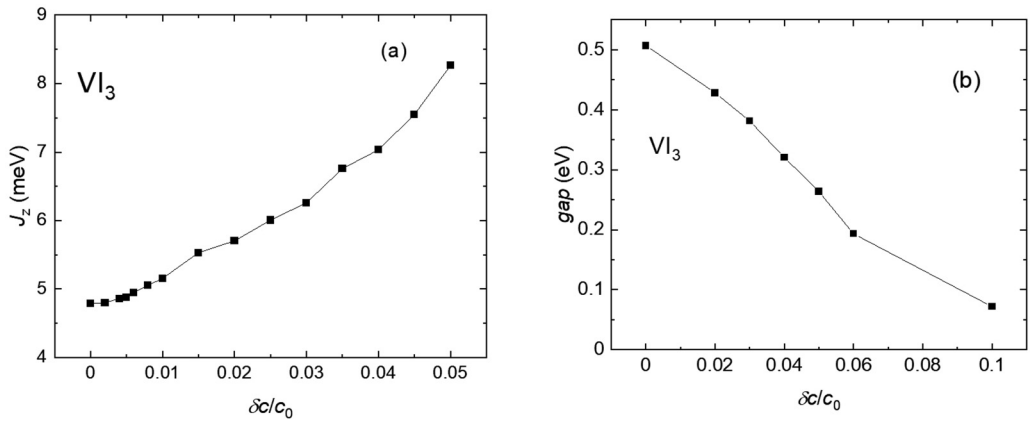

FIG. 12. Calculated dependence of the exchange coupling $J_z = E_{FM} - E_{zAFM}$ (a) and the energy gap (b) on the relative compression of the VI_3 single crystal along the c^* axis.

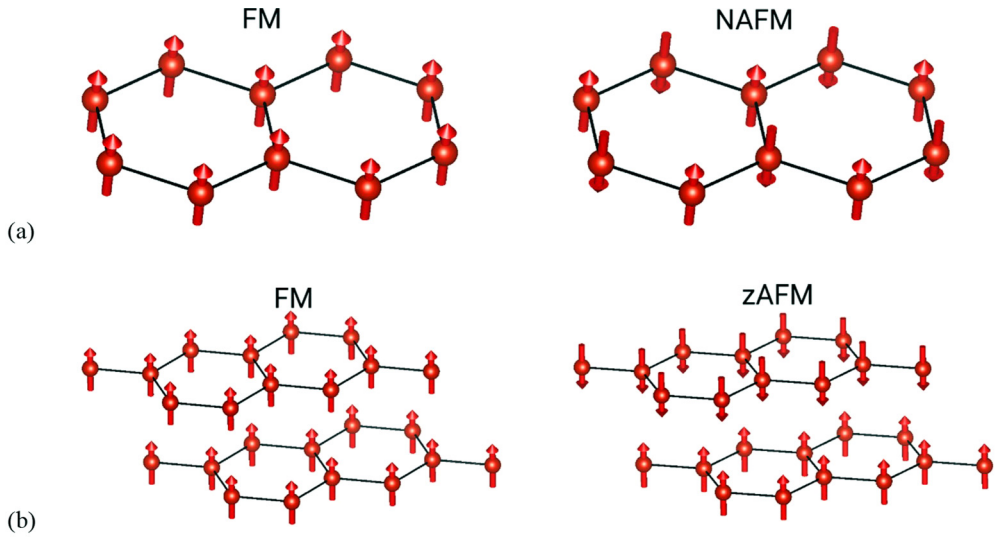

FIG. 13. Possible magnetic orders relevant for determination of magnetic interactions and Curie temperatures: (a) within one layer (b) between layers.

loops up to 0.78 GPa is shown in Figs. 16 and 17 and the extended measurements to 7.3 GPa are shown in Fig. 18 in the Appendix. There we can see that the c^* axis magnetization in high fields decreases with increasing pressure by almost the same rate as in the lower-pressure measurements performed with the 1 GPa piston-cylinder cell. If this reduction in the measured magnetization is proportional to the change in the magnetic moment of the ion V, it would mean that the V moment decreases to half of its ambient-pressure value due to the application of $p = 2.5$ GPa [see also Fig. 15(c)]. Such an effect of pressure on the magnetic moment of vanadium is challenging to imagine in insulators. The rate of moment reduction for field along the c^* axis is higher than that in perpendicular direction. This may indicate an increasing angle of canting of moments from the c^* axis with increasing pressure between 0 and 2.5 GPa.

The high-field magnetization decreases at a very similar rate in pressures up to 2.5 GPa. At higher pressures from 3.4 to 7.3 GPa, it almost does not change. It may be connected with the nonhydrostaticity as mentioned above of pressure due to the frozen medium in DAC in this pressure range. In this case, preferentially uniaxial stress along the c^* axis is expected, whereas the in-ab-plane compression increment may become negligible. If compression in the *ab* plane has a dominant effect on the V magnetic moment, the uniform magnetization can be understood at the highest pressures.

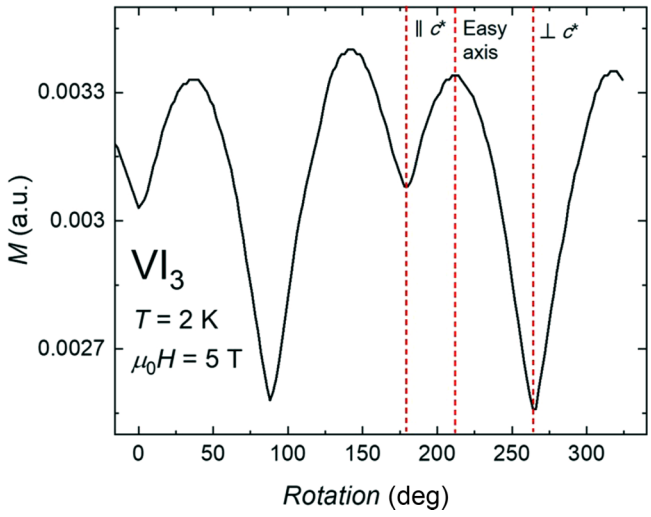

FIG. 14. Angular dependence of the ambient-pressure magnetization in the c^*-a plane of a VI_3 single crystal at 2 K.

An explanation of this result would be possible in case of pressure-induced delocalization of the 3 d electrons and some kind of metallization of VI_3 slowly progressing already from low pressures, which is, however, highly unlikely. Our calculations show that the interlayer distance compression leads to a linear decrease of the bandgap (Fig. 12), which would finally close if the interlayer distance c would be reduced by $\delta c \sim 0.1 c_0$, where c_0 is the equilibrium interlayer distance. Pressure-induced insulator-metal transition can thus be expected, but not at low pressures.

The discovery of a pressure-induced insulator-metal transition in a vdW compound $FePS_3$ accompanied by a transition from ambient-pressure AFM to high-pressure metallic ferromagnetism was recently published [35]. The thorough study by x-ray and neutron diffraction revealed a complex pressure AFM → FM transformation (evolution), composed of several stages extended to much lower pressures than the critical pressure of the Mott transition [35,36]. Therefore, we feel that the puzzle of the pressure-induced evolution of V magnetic moments can be resolved only after a thorough study based on x-ray and neutron diffraction and possibly muon spin spectroscopy studies.

V. CONCLUSIONS

In this study we have observed four magnetic phase transitions at temperatures $T_1 = 54.5$ K, $T_2 = 53$ K, $T_C = 49.5$ K, and $T_{FM} = 26$ K, respectively. The upper two transitions are attributed to the onset of ferromagnetism in the crystal-surface layers caused by a deficiency of iodine or some specific lattice

defects preceding the crystal surface's decomposition. The Curie temperature of the bulk ferromagnetism is seen in a λ-shaped anomaly of the temperature dependence of specific heat and relevant experiments. The temperature T_{FM} is a characteristic of a transition between two different ferromagnetic phases, which is accompanied by a structure transition from monoclinic to triclinic symmetry upon cooling. The first three transitions are only slightly affected by pressures up to 0.6 GPa, whereas the T_{FM} transition moves quickly to higher temperatures with increasing pressure. Only one magnetic (ferromagnetic) phase transition at 55.5 K is observed in pressures > 0.9 GPa. T_C then further increases with increasing pressure. The $T_C(p)$ increase almost saturates around 2.5 GPa. A rapid increase of T_C is restored in pressures above 3 GPa to reach 99 K at 7.3 GPa. In contrast to increasing T_C, the low-temperature bulk magnetization is significantly reduced by pressures up to 2.5 GPa, indicating a possible pressure-induced reduction of vanadium magnetic moment. The results are discussed in recent publications including the theoretical studies that analyzed exchange interactions and suggested ways to increase the Curie temperature of VI_3.

A thorough study of crystal structure and microscopic aspects of magnetism by x-ray and neutron diffraction and possibly μSR spectroscopy studies of the VI_3 single crystals under pressure is needed to resolve the mechanism responsible for the results presented in this paper.

ACKNOWLEDGMENTS

This work is part of the research program GACR 19–16389J which is financed by the Czech Science Foundation. Work at SNU was supported by the Leading Researchers Program of the National Research Foundation of Korea [Grant No. 2020R1A3B2079375] and by the Institute for Basic Science [Grant No. IBS-R009-G1] of the Republic of Korea. Experiments were performed in MGML (Ref. [52]), which is supported within the program of Czech Research Infrastructures (Project No. LM2018096).

APPENDIX: THE HYSTERESIS LOOPS

The hysteresis loops of VI_3 single crystals were measured in magnetic fields applied parallel and perpendicular to the c^* axis both at ambient conditions and at hydrostatic pressures using various types of pressure cells covering crucial parts of the T-p phase space. The $M(H)$ measurement performed with the 1 GPa piston-cylinder cell shows decreasing magnetization with increasing pressure (see Fig. 15). The temperature evolution of the hysteresis loops at ambient conditions is shown in Fig. 16 and at hydrostatic pressures up to 0.78 GPa in Fig. 17. The extended measurements to 7.3 GPa measured using the DAC at low temperatures are shown in Fig. 18.

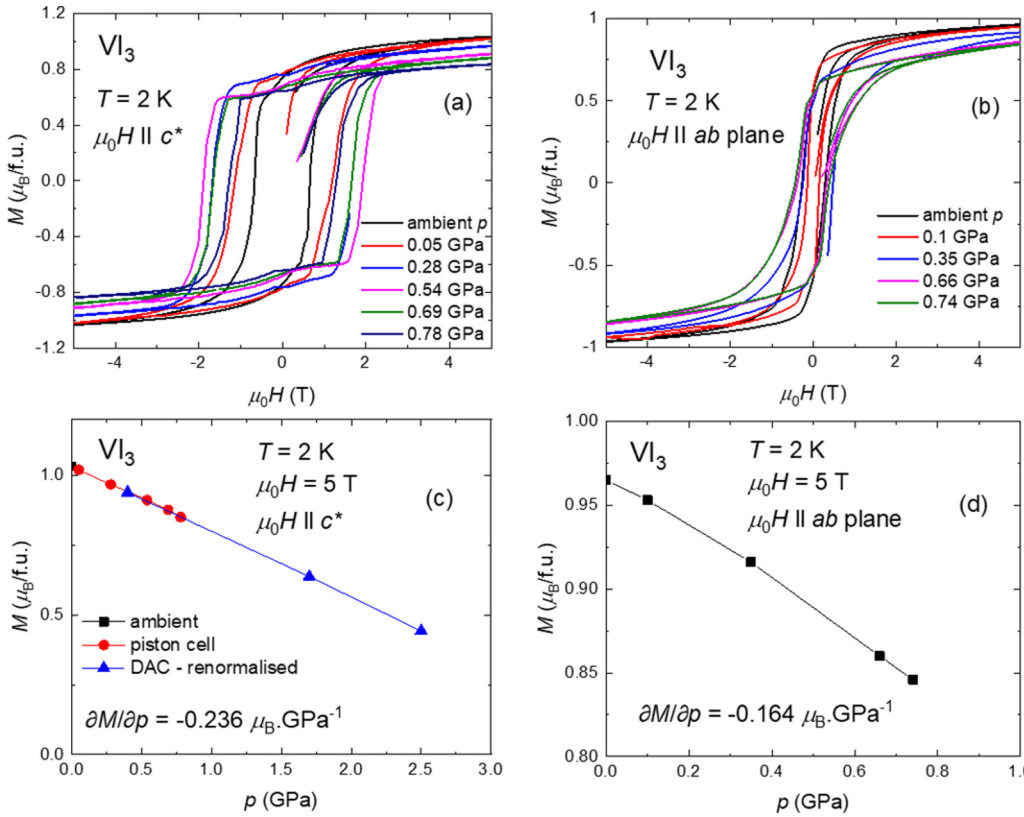

FIG. 15. Magnetization hysteresis loops of a VI_3 crystal exposed to several hydrostatic pressures measured at 2 K in magnetic fields applied parallel (a) and perpendicular (b) to the c^* axis. Pressure dependence of the magnetic moment of VI_3 measured at 2 K in the magnetic field of 5 T applied parallel (c) and perpendicular (d) to the c^* axis.

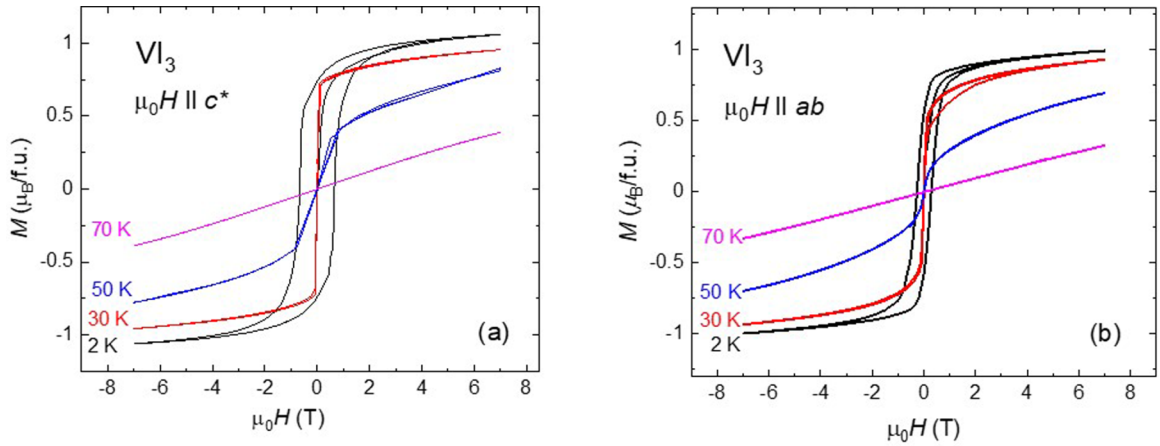

FIG. 16. Magnetization hysteresis loops of a VI_3 crystal measured in ambient pressure at 2 K in magnetic fields applied along (a) and perpendicular (b) to the c^* axis.

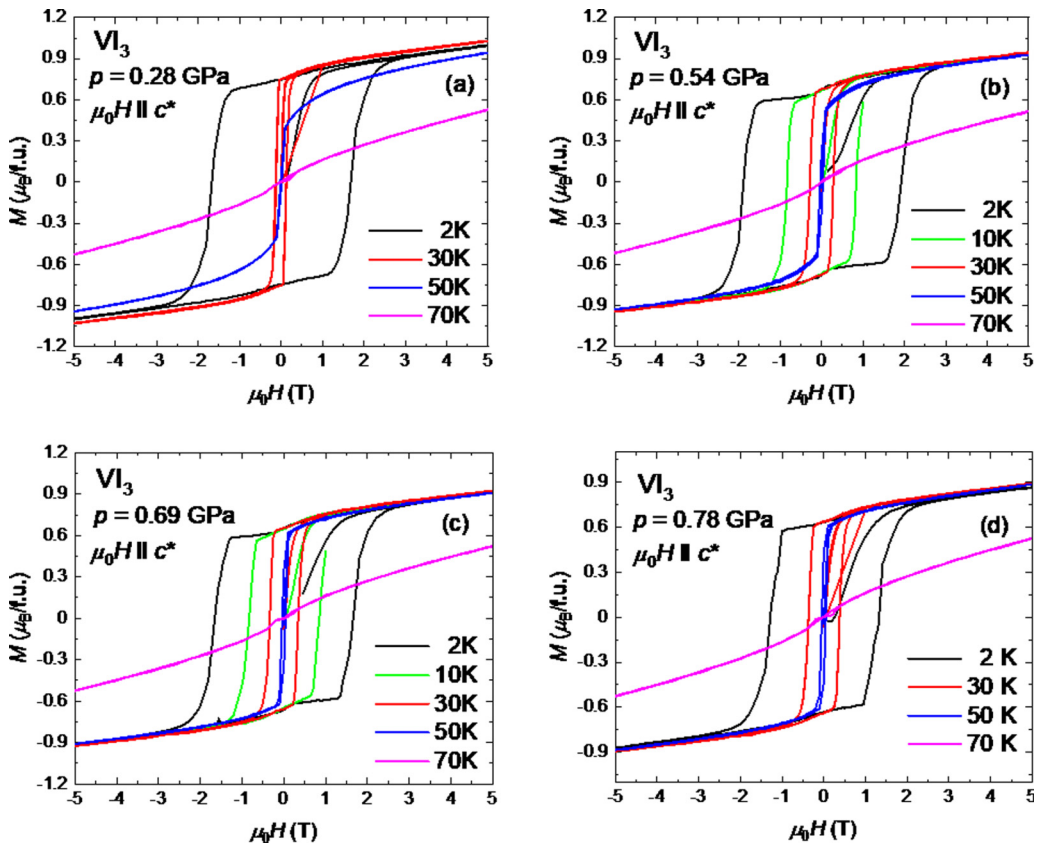

FIG. 17. Magnetization hysteresis loops of a VI_3 crystal measured at 2, 30, 50, and 70 K, respectively, in hydrostatic pressure of 0.28 GPa (a), 0.54 GPa (b), 0.69 GPa (c) and 0.78 GPa (d) in the magnetic field applied along the c^* axis.

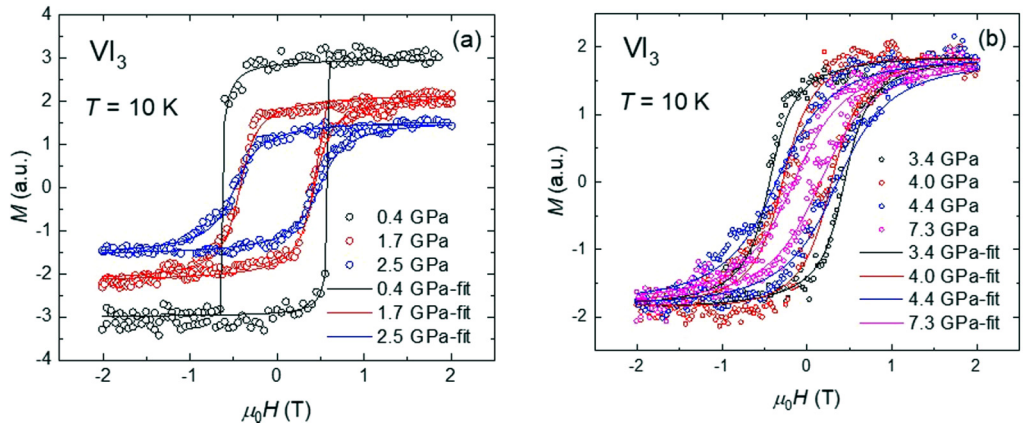

FIG. 18. Magnetization hysteresis loops of a VI_3 crystal measured at 10 K in the magnetic field applied along the c^* axis at pressures: (a) 0.4, 1.7, and 2.5 GPa; (b) 3.4, 4.0, 4.4, and 7.3 GPa.

[1] P. Ajayan, P. Kim, and K. Banerjee, Phys. Today **69**(9), 39 (2016).

[2] K. S. Burch, D. Mandrus, and J. G. Park, Nature (London) **563**, 47 (2018).

[3] J. G. Park, J. Phys.: Condens. Matter **28**, 301001 (2016).

[4] M. Gibertini, M. Koperski, A. F. Morpurgo, and K. S. Novoselov, Nat. Nanotechnol. **14**, 408 (2019).

[5] S. Son, M. J. Coak, N. Lee, J. Kim, T. Y. Kim, H. Hamidov, H. Cho, C. Liu, D. M. Jarvis, P. A. C. Brown, J. H. Kim, C. H. Park, D. I. Khomskii, S. S. Saxena, and J.-G. Park, Phys. Rev. B **99**, 041402(R) (2019).

[6] T. Kong, K. Stolze, E. I. Timmons, J. Tao, D. R. Ni, S. Guo, Z. Yang, R. Prozorov, and R. J. Cava, Adv. Mater. **31**, 1808074 (2019).

[7] S. J. Tian, J. F. Zhang, C. H. Li, T. P. Ying, S. Y. Li, X. Zhang, K. Liu, and H. C. Lei, J. Am. Chem. Soc. **141**, 5326 (2019).

[8] E. Gati, Y. Inagaki, T. Kong, R. J. Cava, Y. Furukawa, P. C. Canfield, and S. L. Bud'ko, Phys. Rev. B **100**, 094408 (2019).

[9] P. Doležal, M. Kratochvílová, V. Holý, P. Čermák, V. Sechovský, M. Dušek, M. Míšek, T. Chakraborty, Y. Noda, S. Son, and J.-G. Park, Phys. Rev. Mater. **3**, 121401(R) (2019).

[10] J. Yan, X. Luo, F. C. Chen, J. J. Gao, Z. Z. Jiang, G. C. Zhao, Y. Sun, H. Y. Lv, S. J. Tian, Q. W. Yin, H. C. Lei, W. J. Lu, P. Tong, W. H. Song, X. B. Zhu, and Y. P. Sun, Phys. Rev. B **100**, 094402 (2019).

[11] Y. Liu, M. Abeykoon, and C. Petrovic, Phys. Rev. Res. **2**, 013013 (2020).

[12] B. Lyu, Y. Gao, Y. Zhang, L. Wang, X. Wu, Y. Chen, J. Zhang, G. Li, Q. Huang, N. Zhang, Y. Chen, J. Mei, H. Yan, Y. Zhao, L. Huang, and M. Huang, Nano Lett. **20**, 6024 (2020).

[13] Y. M. Wang, S. J. Tian, C. H. Li, F. Jin, J. T. Ji, H. C. Lei, and Q. M. Zhang, Chin. Phys. B **29**, 056301 (2020).

[14] A. K. Kundu, Y. Liu, C. Petrovic, and T. Valla, Sci. Rep. **10**, 15602 (2020).

[15] M. An, Y. Zhang, J. Chen, H. M. Zhang, Y. J. Guo, and S. Dong, J. Phys. Chem. C **123**, 30545 (2019).

[16] K. Yang, F. Fan, H. Wang, D. I. Khomskii, and H. Wu, Phys. Rev. B **101**, 100402(R) (2020).

[17] F. Subhan and J. S. Hong, J. Phys.: Condens. Matter **32**, 245803 (2020).

[18] Y. Lee, T. Kotan, and L. Q. Ke, Phys. Rev. B **101**, 241409(R) (2020).

[19] Y. L. Ren, Q. Q. Li, W. H. Wan, Y. Liu, and Y. F. Ge, Phys. Rev. B **101**, 134421 (2020).

[20] M. Baskurt, I. Eren, M. Yagmurcukardes, and H. Sahin, Appl. Surf. Sci. **508**, 144937 (2020).

[21] C. Long, T. Wang, H. Jin, H. Wang, and Y. Dai, J. Phys. Chem. Lett. **11**, 2158 (2020).

[22] Z. P. Guo, Q. Chen, J. N. Yuan, K. Xia, X. M. Wang, and J. Sun, J. Phys. Chem. C **124**, 2096 (2020).

[23] Y. P. Wang and M. Q. Long, Phys. Rev. B **101**, 024411 (2020).

[24] C. X. Huang, F. Wu, S. L. Yu, P. R. Jena, and E. J. Kan, Phys. Chem. Chem. Phys. **22**, 512 (2020).

[25] F. Subhan and J. S. Hong, J. Phys. Chem. C **124**, 7156 (2020).

[26] J. J. He, S. Y. Ma, P. B. Lyu, and P. Nachtigall, J. Mater. Chem. C **4**, 2518 (2016).

[27] J. Yang, J. Wang, R. Liu, Q. Xu, Y. Li, M. Xia, Z. Li, and F. Gao, Appl. Surf. Sci. **524**, 146490 (2020).

[28] B. Huang, G. Clark, E. Navarro-Moratalla, D. R. Klein, R. Cheng, K. L. Seyler, D. Zhong, E. Schmidgall, M. A. McGuire, D. H. Cobden, W. Yao, D. Xiao, P. Jarillo-Herrero, and X. D. Xu, Nature (London) **546**, 270 (2017).

[29] M. A. McGuire, H. Dixit, V. R. Cooper, and B. C. Sales, Chem. Mater. **27**, 612 (2015).

[30] H. Rydberg, M. Dion, N. Jacobson, E. Schroder, P. Hyldgaard, S. I. Simak, D. C. Langreth, and B. I. Lundqvist, Phys. Rev. Lett. **91**, 126402 (2003).

[31] H. D. Flack, J. Appl. Crystallogr. **5**, 137 (1972).

[32] R. W. Lynch and H. G. Drickame, J. Chem. Phys. **44**, 181 (1966).

[33] R. M. Hazen and L. W. Finger, Am. Mineral. **63**, 293 (1978).

[34] M. O. Filso, E. Eikeland, J. Zhang, S. R. Madsen, and B. B. Iversen, Dalton Trans. **45**, 3798 (2016).

[35] C. R. S. Haines, M. J. Coak, A. R. Wildes, G. I. Lampronti, C. Liu, P. Nahai-Williamson, H. Hamidov, D. Daisenberger, and S. S. Saxena, Phys. Rev. Lett. **121**, 266801 (2018).

[36] M. J. Coak, D. M. Jarvis, H. Hamidov, A. R. Wildes, J. A. M. Paddison, C. Liu, C. R. S. Haines, N. T. Dang, S. E. Kichanov, B. N. Savenko, S. Lee, M. Kratochvilova, S. Klotz, T. Hansen, D. P. Kozlenko, J. G. Park, and S. S. Saxena, Phys. Rev. X (to be published), arXiv:2008.11447v1.

[37] J. Kamarad, Z. Machatova, and Z. Arnold, Rev. Sci. Instrum. **75**, 5022 (2004).

[38] S. Sasaki, S. Kato, T. Kume, H. Shimizu, T. Okada, S. Aoyama, F. Kusuyama, and K. Murata, Jpn. J. Appl. Phys. **49**, 106702 (2010).

[39] G. Giriat, W. W. Wang, J. P. Attfield, A. D. Huxley, and K. V. Kamenev, Rev. Sci. Instrum. **81**, 073905 (2010).

[40] D. Stasko, J. Prchal, M. Klicpera, S. Aoki, and K. Murata, High Pressure Research **40**, 525 (2020).

[41] M. Misek, J. Prokleska, V. Sechovsky, D. Turcinkova, J. Prchal, A. F. Kusmartseva, K. V. Kamenev, and J. Kamarad, J. Appl. Phys. **111**, 07E132 (2012).

[42] M. Nikolo, Am. J. Phys. **63**, 57 (1995).

[43] K. Murata, H. Yoshino, H. O. Yadav, Y. Honda, and N. Shirakawa, Rev. Sci. Instrum. **68**, 2490 (1997).

[44] http://elk.sourceforge.net/.

[45] V. I. Anisimov, J. Zaanen, and O. K. Andersen, Phys. Rev. B **44**, 943 (1991).

[46] S. Mondal, M. Kannan, M. Das, L. Govindaraj, R. Singha, B. Satpati, S. Arumugam, and P. Mandal, Phys. Rev. B **99**, 180407(R) (2019).

[47] H. Yoshida, J. Chiba, T. Kaneko, Y. Fujimori, and S. Abe, Physica B **237**, 525 (1997).

[48] A. O. Fumega, S. Blanco-Canosa, H. Babu-Vasili, V. Gargiani, H. Li, J. S. Zhou, F. Rivadulla, and V. Pardo, J. Mater. Chem. C **8**, 13582 (2020).

[49] X. Wang, Z. Li, M. Zhang, T. Hou, J. Zhao, L. Li, A. Rahman, Z. Xu, J. Gong, Z. Chi, R. Dai, Z. Wang, Z. Qiao, and Z. Zhang, Phys. Rev. B **100**, 014407 (2019).

[50] J. L. Lado and J. Fernandez-Rossier, 2d Materials **4**, 035002 (2017).

[51] D. H. Kim, K. Kim, K. T. Ko, J. H. Seo, J. S. Kim, T. H. Jang, Y. Kim, J. Y. Kim, S. W. Cheong, and J. H. Park, Phys. Rev. Lett. **122**, 207201 (2019).

[52] https://mgml.eu/.